[superscript 2]H-DNP-enhanced [superscript 2]H-[superscript 13]C solid-state NMR correlation spectroscopy

ARTICLE TYPE www.rsc.org/xxxxxx | XXXXXXXX

^{2}H-DNP-enhanced ^{2}H-^{13}C solid-state NMR correlation spectroscopy

Thorsten Maly, Loren B. Andreas and Robert G. Griffin*

Received (in XXX, XXX) Xth XXXXXXXXX 200X, Accepted Xth XXXXXXXXX 200X
First published on the web Xth XXXXXXXXX 200X
DOI: 10.1039/b000000x

Perdeuteration of biological macromolecules for magic angle spinning solid-state NMR spectroscopy can yield high-resolution ^{2}H-^{13}C correlation spectra and the method is therefore of great interest for the structural biology community. Here we demonstrate that the combination of sample deuteration and dynamic nuclear polarization yields resolved ^{2}H, ^{13}C correlation spectra with a signal enhancement of $\varepsilon \geq 700$ compared to a spectrum recorded with microwaves off and otherwise identical conditions. To our knowledge, this is the first time that ^{2}H-DNP has been employed to enhance MAS-NMR spectra of a biologically relevant system. The DNP process is studied using several polarizing agents and the technique is applied to obtain ^{2}H-^{13}C correlation spectra of U-[^{2}H, ^{13}C] proline.

Introduction

In recent years magic angle spinning NMR (MAS-NMR) spectroscopy has emerged as a valuable method to determine atomic-resolution structures of biomolecular macromolecules such as globular proteins, membrane proteins and amyloid fibrils [1, 2]. However, in contrast to solution-state NMR, the majority of MAS-NMR experiments rely on recording homo- and heteronuclear ^{13}C and ^{15}N correlation spectra because direct ^{1}H detection is often compromised by the strong ^{1}H-^{1}H dipolar interactions present in the solid state. Under typical experimental conditions, these strong couplings result in broad, unresolved ^{1}H resonances. Techniques such as ultrafast sample spinning [3, 4], windowed homonuclear decoupling techniques [5, 6], and dilution of the ^{1}H-^{1}H dipolar bath by deuteration can be used to narrow ^{1}H lines in MAS-NMR experiments and are currently under investigation [7-10]. Successful implementation of these techniques would bring the resolving power of a third nucleus to MAS-NMR protein investigations.

Another approach to access a third nucleus is to observe deuterons (^{2}H) because their reduced homonuclear dipolar coupling that can be attenuated under moderate MAS frequencies (~ 5 kHz). Deuterons contain similar information on the chemical environment as protons, and can therefore be directly employed to obtain structural information.

Recently it was shown that spectra of deuterated proteins exhibit high-resolution MAS-NMR spectra and the method is therefore of great interest for the structural biology community [8, 11]. Furthermore, deuteration can also result in additional benefits in both the resolution and sensitivity of more conventional ^{13}C and ^{15}N MAS-NMR experiments. For example, the resolution of 3D or 4D ^{13}C spectra of deuterated proteins is no longer limited by the ^{1}H decoupling power and resulting rf heating. In addition, cross-polarization (CP) enhancements are increased and neither ^{1}H nor ^{13}C longitudinal relaxation times are significantly increased [12]. However, the ^{2}H quadrupole coupling (e^2qQ/h ~167 kHz for a CD bond) often reduces the sensitivity and resolution of directly observed ^{2}H spectra in solids. At the same time, the relaxation and lineshape properties of the deuterium nucleus are particularly sensitive to the local dynamics and can provide valuable information [8].

To overcome the difficulties associated with the deuterium quadrupole coupling, techniques such as rotor-synchronized pulse sequences or indirect detection through for example ^{13}C can be used. Furthermore, in hetero-nuclear correlation experiments (e.g. ^{2}H-^{13}C), MAS narrows the first order ^{2}H quadrupole interaction and the resolution can be further improved if a ^{2}H double-quantum (^{2}H-DQ) excitation and reconversion scheme is employed [11, 13, 14].

NMR signal intensities of solids and liquids can be enhanced by several orders of magnitude with dynamic nuclear polarization (DNP) [15, 16] and in the last decade high-frequency DNP has emerged as a valuable method for a variety of applications, spanning particle physics [17, 18], pharmaceutical applications [19, 20] and structural and mechanistic studies of biologically relevant molecules [15, 21, 22].

In a DNP experiment, the large thermal polarization of a paramagnetic polarizing agent is transferred to surrounding nuclei by microwave irradiation of the sample at the electron paramagnetic resonance (EPR) transition. DNP enhancements are measured by taking the ratio of signal intensity in spectra with and without microwaves, leaving all other experimental parameters unchanged. Depending on the inhomogeneous breadth of the EPR spectrum (Δ) and the homogeneous linewidth (δ), DNP can either occur through the solid-effect (SE) if the nuclear Larmor frequency ω_{0I} is larger than the EPR linewidth ($\omega_{0I} > \Delta, \delta$), or through the much more efficient cross-effect (CE) if $\Delta > \omega_{0I} > \delta$ [15, 25]. In the classical description of the CE the underlying mechanism is a two-step process involving two electrons with Larmor frequencies ω_{0S1} and ω_{0S2}, and a nucleus with a frequency ω_{0I}. Initially, the *allowed* EPR transition of one electron is irradiated and

nuclear polarization is generated in a subsequent three-spin flip-flop process through transitions such as $|\alpha_{1S}\beta_{2S}\beta_I\rangle \leftrightarrow |\beta_{1S}\alpha_{2S}\alpha_I\rangle$ or $|\beta_{1S}\alpha_{2S}\beta_I\rangle \leftrightarrow |\alpha_{1S}\beta_{2S}\alpha_I\rangle$ [26, 27]. The maximum DNP enhancement is achieved when the difference between the electron Larmor frequencies of two electron spin packets satisfy the matching condition $|\omega_{0S1} - \omega_{0S2}| = \omega_{0I}$, with ω_{0I} the nuclear Larmor frequency. The DNP-enhanced nuclear polarization then disperses throughout the bulk via spin-diffusion.[28] Currently, the largest signal enhancements in solids at high magnetic fields (>5 T) are observed in experiments where the cross-effect (CE) is the dominant DNP mechanism [23, 24].

Here we demonstrate that the combination of sample deuteration and DNP yields resolved ^{2}H, ^{13}C correlation spectra with a signal enhancement of $\varepsilon \geq 700$. To our knowledge, ^{2}H-DNP has been reported only for the preparation of polarized targets [29-31] and in dissolution DNP [32], focusing on the polarization of small alcohol molecules. In this study, we demonstrate that high-field ^{2}H-DNP can be used to enhance MAS-NMR spectra of biologically relevant molecules. Although the technique is initially demonstrated using a single amino acid residue, the concept has considerable potential for structural investigations of biologically relevant macromolecules in the solid state at high magnetic fields. Given sufficient sensitivity, the resolving power of ^{2}H, ^{13}C and ^{15}N, 3D and 4D experiments have the potential to extend MAS-NMR to the application of larger biological systems.

Results and Discussion

Polarizing Agents and DNP-Enhancement Profiles

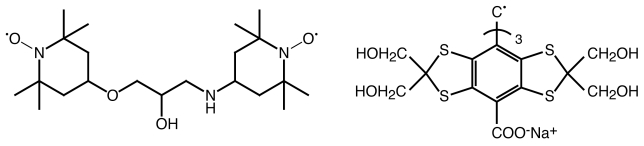

Figure 1: Molecular structures of the two polarizing agents TOTAPOL and OX063.

The molecular structures of the two polarizing agents TOTAPOL (1-(TEMPO-4-oxy)-3-(TEMPO-4-amino)-propan-2-ol) and OX063 (methyl-tris[8-carboxy-2,2,6,6-tetrakis[(2-hydroxyethyl]-benzo[1,2-d:4,5-d]bis[1,3]dithiol-4-yl]) are shown in **Figure 1** and both are soluble in aqueous media at high concentration.

The 140 GHz (5 T) EPR spectra of TOTAPOL and OX063 are shown in **Figure 2** (top). While the EPR spectrum of TOTAPOL shows a large g-anisotropy and additional features due to the ^{14}N hyperfine interaction with the electron spin [33], the EPR spectrum of OX063 appears almost symmetric at high-magnetic fields because no significant hyperfine couplings are present and the g-tensor anisotropy is small[34]. With an inhomogeneous breadth of $\Delta \approx 600$ MHz and 55 MHz for TOTAPOL and OX063, respectively, and a ^{2}H nuclear Larmor frequency at 5 T of 32 MHz, we see that both radicals satisfy the conditions ($\Delta > \omega_{0I} > \delta$) for CE DNP for ^{2}H.

The field swept DNP enhancement profile is closely related to the high-field EPR spectrum recorded at the same magnetic field strengths as shown in **Figure 2**. Typically high-field DNP experiments are performed using a fixed-frequency microwave source and the DNP process needs to be optimized with respect to the magnetic field to find the best irradiation frequency.

In addition to determining the optimum field position for DNP, the enhancement profile also reveals much information about the nature of the underlying DNP process. Since both enhancement profiles of TOTAPOL and OX063 do not show resolved features at frequencies corresponding to $\omega_{0S} \pm \omega_{0I}$, it can be directly concluded that the underlying DNP mechanism observed in experiments reported here is the CE [18, 25, 27, 35-37].

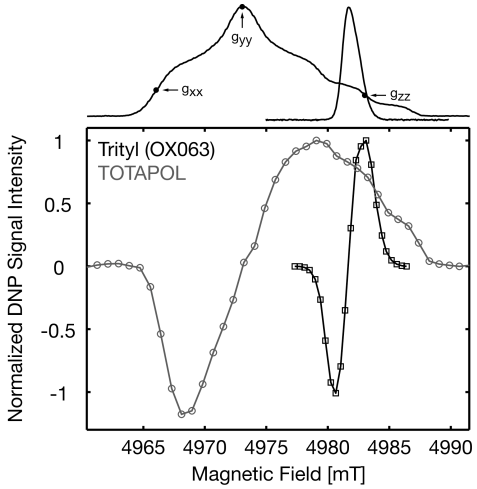

Figure 2: Top: Two-pulse echo-detected 140 GHz EPR spectra of 1 mM TOTAPOL and OX063 in glycerol/H_2O (60/40), T = 20 K. Bottom: Direct detected ^{2}H-DNP enhancement profiles of 20 mM TOTAPOL and 40 mM Trityl (OX063) in d_8-glycerol/D_2O (60/40) using a rotor-synchronized quadrupole-echo sequence. T = 90 K, $t_p(\pi/2) = 3$ µs, $\tau = 166$ µs, $\omega_r/2\pi = 6$ kHz. For comparison the DNP enhancement profiles are normalized to maximum intensity.

The DNP enhancement profile for TOTAPOL resembles the shape typically observed for TEMPO based (bi)-radicals [38-40]. For ^{2}H-DNP the maximum negative enhancement is obtained at the low-field side of the profile corresponding to 4968.6 mT (DNP(-)), while the maximum positive enhancement is observed at 4979.1 mT (DNP(+)). This is in contrast to ^{1}H-DNP, where the overall extremum ^{1}H enhancement is observed at the high-field side (DNP(+)) of the DNP enhancement profile [38, 41]. Note that the ^{2}H-DNP enhancement profile for TOTAPOL shows a pronounced asymmetry. This feature is similar to direct ^{13}C-DNP using TOTAPOL and the two enhancement profiles for ^{2}H and ^{13}C DNP coincide with the maximum absolute enhancement observed on the low-field side (DNP(-)). This appears to be an inherent feature of TEMPO based polarizing agents, when low-γ nuclei such as ^{13}C and ^{2}H are polarized. In contrast to ^{1}H-DNP the maximum absolute enhancement is observed on the high-field side (DNP(+)).

For ^{1}H DNP, the TEMPO based biradical TOTAPOL currently yields the largest enhancements in DNP-enhanced MAS-NMR experiments [38, 41]. However, with an inhomogeneous breadth of $\Delta \approx 600$ MHz at 5 T, TOTAPOL is

not optimized for polarizing low-γ nuclei such as ^{2}H, ^{13}C or ^{15}N and polarizing agents with narrower EPR spectra are preferable. At present only two radicals are known for DNP applications that have a narrow EPR spectrum at high magnetic fields, the stable trityl radical and its derivatives [42, 43] and BDPA [44]. Here we choose the trityl radical OX063 (see **Figure 1**) as the polarizing agent, because of its copious solubility in aqueous media [45]. The 140 GHz EPR spectrum of OX063 is shown in **Figure 2** (top). The spectrum is essentially symmetric with a spectral breadth of $\Delta \approx 55$ MHz (FWHH) as determined from the EPR spectrum. As a consequence the enhancement profile of OX063 for direct ^{2}H-DNP shown in **Figure 2** is symmetric with the maximum positive enhancement occurring at 4983.0 mT (DNP(+)) and the maximum negative enhancement occurring at 4980.7 mT (DNP(-)).

A direct comparison of these two enhancement profiles can be used to illustrate another important fact for high-field DNP. At 5 T the separation between the optimum field positions for ^{1}H-DNP using TOTAPOL (DNP(+)) and ^{2}H-DNP (or ^{13}C) is approximately 4 mT, corresponding to ~ 112 MHz electron Larmor frequency. The separation is 14 mT between DNP(-) for TOTAPOL and DNP(+) for OX063, corresponding to 400 MHz for electrons. To be able to study different polarizing agents and to cover the complete field range, the DNP spectrometer has to be equipped either with a sweep coil or the gyrotron needs to be tunable over a range of > 0.5 GHz [46-48]. Note that the sweep/tuning range will increase at higher fields.

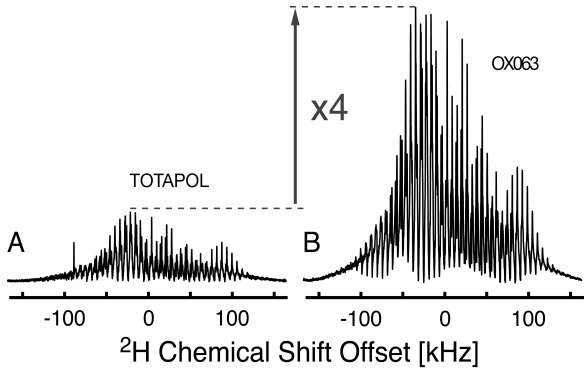

Figure 3: Comparison of the steady-state ^{2}H signal intensity for TOTAPOL (A) and OX063 (B). Both spectra are recorded back-to-back under identical experimental conditions. Due to the insufficient excitation bandwidth of 83 kHz, the magnitude spectrum is shown. T = 90 K, $\omega_r/2\pi = 5.882$ kHz. The spectra are recorded using a rotor-synchronized quadrupole echo sequence.

A comparison of the ^{2}H-DNP performance for TOTAPOL and OX063 is shown in **Figure 3** and approximately a factor of 4 larger enhancement is observed for OX063 under similar experimental conditions. This improvement is due to the much narrower EPR spectrum of OX063 (Δ(TOTAPOL)/Δ(OX063) ≈ 11) allowing a larger fraction of the electron spins to be excited by the microwave radiation. Note that at the same electron concentration TEMPO based biradicals give a factor of 4 larger enhancements compared to monomeric TEMPO [23], and we therefore expect that further improvements could be made using biradicals based on OX063. Due to the much better performance of OX063 over TOTAPOL, the following DNP experiments were all performed using OX063 as the polarizing agent.

Bulk-Polarization Build-up and Maximum Enhancement

During the DNP process, the high thermal electron polarization is transferred to the surrounding nuclei resulting in a bulk-polarization build-up curve that can be modeled by an exponential process with a characteristic bulk-polarization build-up time constant τ_B. **Figure 4** illustrates a ^{13}C-detected bulk-polarization build-up curve for ^{2}H DNP using OX063 as the polarizing agent. Here the DNP-enhanced ^{2}H polarization is transferred to the proline ^{13}C nuclei for detection via a subsequent cross-polarization (CP) step [49]. This allows an accurate determination of the signal enhancement, because the ^{13}C spectrum is much narrower compared to the direct detected ^{2}H spectrum. At a temperature of 90 K, the steady state polarization is reached after approximately 100 s of microwave irradiation yielding a build-up time constant of $\tau_B(^{2}H) = 21$ s.

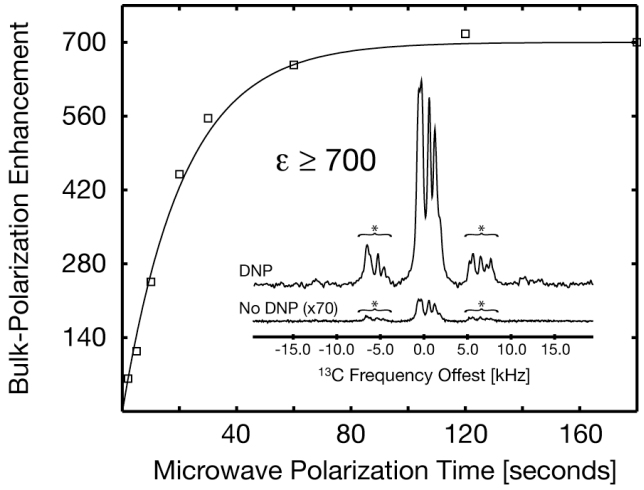

Figure 4: ^{2}H bulk-polarization build-up curve recorded at a magnetic field position corresponding to DNP(+) using OX063. The ^{2}H polarization is detected indirectly from the total ^{13}C signal of U-[$^{2}H_7$, $^{13}C_5$]-proline through a ramped cross-polarization step (1.5 ms), 16 scans averaged. The inset shows the mw-on and off signal. The DNP enhanced spectrum was recorded at a field position corresponding to DNP(+) with a DNP buildup time of $t_{mw} = 120$ s. For the mw-on signal 32 transient were averaged while for the mw-off signal in total 1280 transients were averaged. T = 90 K, $\omega_r/2\pi = 5.882$ kHz. Spinning side bands are marked by asterisks.

The absolute enhancement is calculated from the microwave on and off spectra, recorded under identical experimental conditions (see **Figure 4**, inset). For the off signal, 40 times more scans were averaged to provide sufficient signal-to-noise due to the small ^{2}H signal intensity without DNP enhancement and a steady-state ^{2}H DNP enhancement of $\varepsilon \geq 700$ was observed. Theoretically, the maximum enhancement that can be achieved in a DNP experiment is given by the ratio of the gyromagnetic ratios of the electron and the nucleus that is polarized, here ^{2}H ($\gamma(e^-)/\gamma(^{2}H)$). This gives a theoretical maximum enhancement of 4300 for ^{2}H-DNP.

In **Figure 5** two direct ^{13}C-DNP enhanced spectra of

proline are shown, one spectrum taken without decoupling (A) and one with 83 kHz high-power ^{2}H TPPM decoupling (B) [50]. As expected, no significant difference in resolution was detected between the two acquisition schemes. Therefore, the following experiments were all performed without decoupling of the (residual) ^{1}H or ^{2}H nuclei.

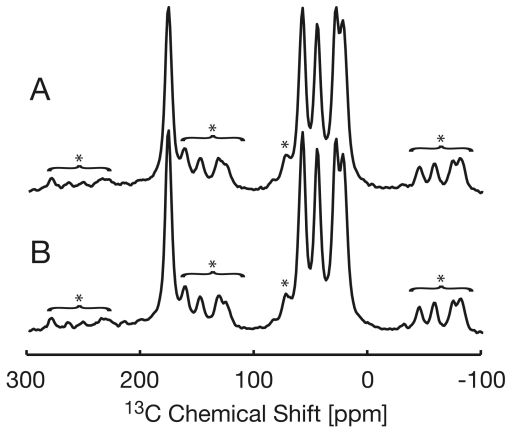

Figure 5: Direct ^{13}C DNP-enhanced MAS-NMR spectra of U-[$^2H_7$, $^{13}C_5$]-proline taken at 90 K, $\omega_R/2\pi$ = 5.5 kHz, 4 scans. A: Spectrum taken without decoupling. B: Spectrum taken with 83 kHz of TPPM ^{2}H decoupling.

^{2}H-DNP Enhanced ^{2}H-^{13}C Correlation Spectroscopy

Depending on the experimental conditions the electron polarization can be either used to polarize ^{13}C nuclei directly ($e^- \rightarrow {}^{13}C$) or indirectly ($e^- \rightarrow {}^2H \rightarrow {}^{13}C$). In the second case the electron polarization is first transferred to the ^{2}H nuclei via DNP and then transferred to the ^{13}C nuclei by a subsequent CP step [51]. In **Figure 6** two ^{2}H-DNP-enhanced ^{13}C detected MAS-NMR spectra of U-[$^2H_7$, $^{13}C_5$]-proline recorded at 90 K are shown. The top spectrum in **Figure 6** is a direct ^{13}C-DNP enhanced spectrum of proline and all five proline ^{13}C resonances are visible. The second spectrum shown in **Figure 6** (bottom) is an indirect polarized ^{13}C spectrum of proline.

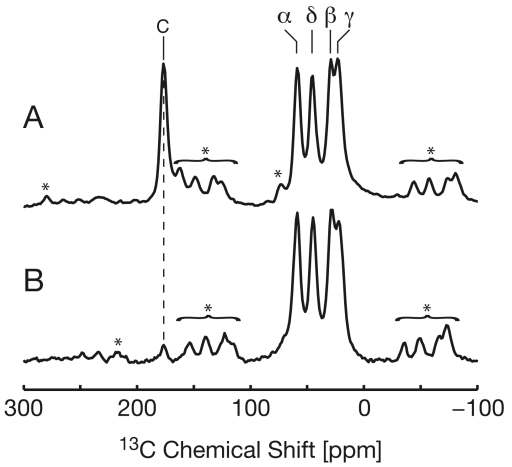

Figure 6: ^{13}C MAS-NMR spectra of U-[$^2H_7$, $^{13}C_5$]-proline taken at 90 K. A: Direct ^{13}C DNP-enhanced MAS-NMR spectrum , $\omega_R/2\pi$ = 5.5 kHz, 4 scans, t_{mw} = 60 s. B: ^{2}H DNP-enhanced ^{13}C MAS-NMR spectrum. The polarization is transferred from ^{2}H to ^{13}C by a cross-polarization step (1.5 ms), $\omega_R/2\pi$ = 5.0 kHz, 64 scans, t_{mw} = 20 s. Spinning side bands are marked by asterisks. The sensitivity of the two spectra are 7.9 and 1.3 S/N•seconds$^{-1/2}$ for A and B, respectively. The main source of sensitivity difference is due to inefficiency in the CP step in which the ^{2}H spin lock of ~83 kHz covers less than half of the ~200 kHz broad ^{2}H spectrum.

Due to the short contact time of the CP process (1.5 ms), predominantly one-bond polarization transfer from ^{2}H to ^{13}C is observed. The ^{13}C signal intensity for the carbonyl atom is attenuated due to the lack of a directly bonded deuterium, whereas nuclei that do posses a directly bonded deuterium (α–γ_i) yield intense lines.

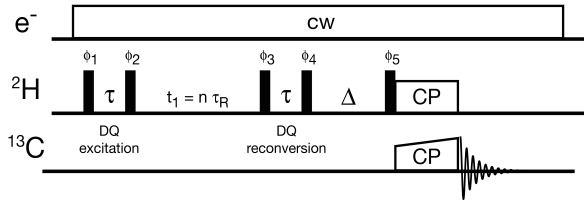

Figure 7: Pulse sequence to record a ^{2}H double-quantum, ^{13}C correlation spectrum. Double quantum coherences are generated using a two-pulse sequence. The t_1 evolution time is rotor-synchronized.

The pulse sequence used for DNP-enhanced ^{2}H double-quantum (DQ) filtered ^{13}C correlation spectroscopy is shown in **Figure 7**. Double quantum coherences are excited using a two-pulse scheme [52], consisting of a DQ excitation and reconversion period (characterized by τ) separated by a rotor-synchronized t_1 evolution period given by $n*\tau_R$ with n the number of rotor cycles and τ_R the rotor period. Finally the ^{2}H magnetization is transferred to ^{13}C by a CP step [51]. For ^{2}H-DNP-enhanced measurements, the sample is irradiated by continuous wave (CW) microwave radiation, on-resonant with the DNP transition.

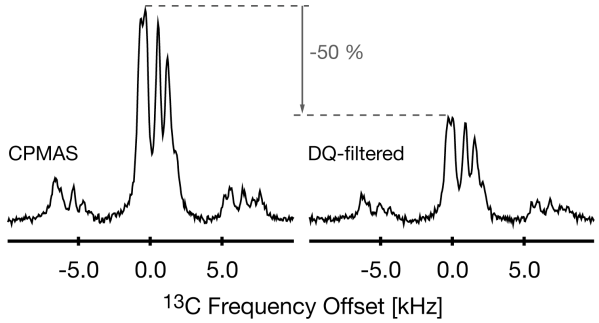

Figure 8: Determination of the DQ efficiency for U-[$^2H_7$, $^{13}C_5$]-proline from DNP enhanced spectra. Top: ^{13}C CPMAS spectrum. Bottom: ^{2}H double-quantum filtered ^{13}C CPMAS spectrum with t_1 = 0. Experimental conditions: T = 90 K, τ = 1 µs, Δ = 3 µs, $\omega_R/2\pi$ = 5.882 kHz, t_{mw} = 20 s.

The DQ efficiency is determined by comparing the signal intensity obtained from a ^{13}C CPMAS experiment with the signal intensity obtained from a ^{2}H double-quantum filtered ^{13}C CPMAS experiment as shown in **Figure 8**. From this comparison a ^{2}H double-quantum efficiency of ~ 50 % is observed.

A two-dimensional ^{2}H-DNP enhanced ^{2}H, ^{13}C correlation spectrum of proline is shown in **Figure 9**. Here a ^{2}H double-quantum filter is used before the polarization is transferred to ^{13}C through a 1.5 ms CP step. A double-quantum excitation and reconversion time of 1 µs was used, followed by a z-filter of 3 µs length. The pulse sequence used here is similar to the

one previously reported for DQ-filtered $^{2}H,^{13}C$ correlation spectroscopy in perdeuterated proteins [11]. The two-dimensional spectrum shows 4 resolved cross-peaks, corresponding to correlations between the ^{13}C proline atoms and the covalently attached ^{2}H nuclei.

Spectral Linewidths

Under the current experimental conditions linewidths of approximately 10 ppm and 8 ppm were observed for ^{2}H and ^{13}C, respectively. These linewidths are larger than those observed previously for perdeuterated proteins [8, 11]. However, the source of the increased linewidth is not of a general nature. In particular the main contribution arises from the fact that proline is a small molecule embedded in a frozen (90 K) glassy solvent matrix (glycerol/water). DNP samples are typically prepared in a glass-forming solvent, which serves as a cryoprotectant to ensure that the polarizing agent is homogenously dispersed throughout the sample and protects proteins from cold degradation caused by thermal cycling of the sample. This is known to induce conformational distributions, which in turn can cause inhomogeneous broadening [53]. However, this factor becomes unimportant for larger systems such as bio-macromolecules or (nano) crystals. For example in contributions by Barnes et al. and Debelouchina et al. (same issue) ^{13}C linewidths of 1-2 ppm are observed for the membrane protein bacteriorhodopsin (bR) and GNNQQNY nanocrystals.

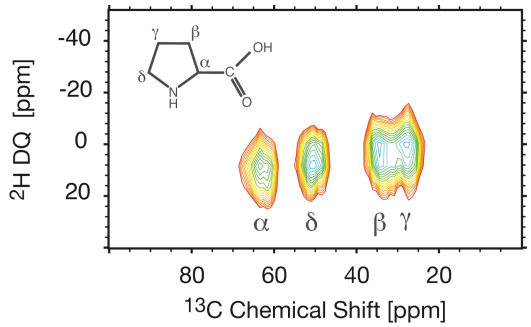

Figure 9: Two-dimensional DNP-enhanced ^{2}H-DQ-^{13}C correlation spectrum of U-[$^{2}H_7$, $^{13}C_5$]-proline recorded at 90 K, $\omega_R/2\pi = 5.882$ kHz, sampling time in the indirect dimension $\Delta t_1 = 170$ µs, DQ excitation and reconversion time $\tau = 1$ µs, $\Delta = 3$ µs, $t_{mw} = 25$ s, 64 scans per t_1 point, ~10 hrs of total acquisition time.

The paramagnetic polarizing agent has only minor effects on the linewidth. For example in DNP-enhanced MAS-NMR experiments on amyloid nanocrystals GNNQQNY [54] or the membrane protein bacteriorhodopsin (bR) the radical does not penetrate into the protein or nanocrystals. In the case of bR even electron concentrations of up to 100 mM did not show any effect on the linewidth of the retinal, which is buried inside the protein [55]. The last factor is of a technical nature. All experiments described here are performed at a magnetic field strength of 5 T (212 MHz for ^{1}H), which is rather low for contemporary MAS-NMR spectroscopy and second order quadrupole effects could have a contribution to the observed linewidth. In addition, it is rather difficult to accurately set the magic angle at cryogenic temperatures for this particular probe, since it is not equipped with a cryogenic sample-eject system [16] or a Hall effect sensor [56]. Although a misadjusted magic angle has only minor effects on the linewidth for double-quantum filtered ^{2}H experiments [11, 14] it nevertheless adds a contribution to the line broadening. There is also the possibility that small inhomogeneities in the magnetic field at the sample caused additional line broadening.

Sensitivity Gain Through DNP

Acquisition of a ^{2}H dimension offers several advantages over a ^{1}H dimension. The deuterium spin system has a lower gyromagnetic ratio, and therefore does not suffer from the homogenous broadening observed for high concentrations of protons in solids. Spins of interest can be perdeuterated without deuteration of solvents, crystallization agents and cofactors. Comparable sensitivity should also be achievable with deuterium detection. For example, methyl-methyl contacts are often important for determination of protein structure, and in cases where a CD_2H labeling is used to reduce proton couplings, perdeuteration (~97%) is employed [8]. At 3% protonation, methyl groups are ~9% CD_2H spin systems to first order, with minimal (~0.3%) CDH_2 and CH_3 labeling. This avoids broadening in the ^{13}C dimension due to the shift in the isotropic resonance between CH and CD which results in different isotropic shifts for CH_3, CH_2D, CHD_2 and CD_3 groups. Since 10% labeling is often found to be necessary for optimized relaxation characteristics of amide protons [8], perdeuteration will be used as a point of comparison, but may need to be adjusted to by a factor of ~3 if higher protonation is found to be optimal.

In a perdeuterated sample (~ 97 %) ^{2}H NMR should have a factor of ~8.6 higher sensitivity compared to ^{1}H detection, and a factor of ~2.5 was experimentally observed by Agarwal et al.. [11]. If CH or CH_2 groups are of primary interest, or if a higher proton concentration is found to be optimal, this analysis needs to be adjusted. This gain in sensitivity is mainly due to the short longitudinal relaxation of the ^{2}H nuclei, a direct consequence of the large quadrupolar coupling. Therefore, at room temperature the recycle delay in the NMR experiment can be short. Furthermore, sample heating is not an issue due to the much lower decoupling power needed for deuterium. Nevertheless recycle delays between 1.25 and 3 s were reported for previous work on biological samples [11].

This advantage no longer exists at 90 K because the DNP build-up time constant is 21 s. Therefore, to run the DNP experiment at the optimum repetition rate one needs to wait 21*1.25 s = 26 s between shots and the sensitivity for low temperature ^{2}H MAS-NMR spectroscopy would be decreased by a factor of 3 to 5 depending on the actual recycle delay used in the experiment compared to experiments performed at 300K. However, the observed DNP signal enhancement of $\varepsilon \geq 700$ leads to an overall sensitivity of a low-temperature ^{2}H-DNP enhanced MAS-NMR experiment that is a factor of 140 to 240 larger than at room temperature. This does not include the additional factor of ~3 in sensitivity due to the lower temperature (300 K/90 K).

To compare the overall efficiency of ^{2}H-DNP with ^{1}H-DNP the degree of nuclear polarization can be compared. In the

case of ^{2}H-DNP this is 16 % of the theoretical maximum, and for ^{1}H-DNP typically 27 % (175/660) is observed at a magnetic field of 5 T [23, 38]. Therefore, overall ^{1}H-DNP currently performs more efficiently than ^{2}H-DNP. However, with further advances in polarizing agents, and despite a bulk-polarization build-up time of ~5 s for ^{1}H-DNP [40] and 21 s for ^{2}H DNP, we expect both methods to be competitive on a sensitivity basis. Importantly, ^{2}H MAS-NMR provides a facile approach to introduce a pseudo-^{1}H dimension into the spectra. Note that this comparison does not include the efficiency of the CP transfer.

Materials and Methods

Sample Preparation

Field swept DNP enhancement profiles are recorded using a solution of 20 mM TOTAPOL or 40 mM OX063 in d_8-glycerol/D_2O (60/40). Direct ^{2}H signal detection was performed using a rotor-synchronized quadrupole-echo sequence.

For DNP experiments on proline, a 1.25 M solution of U-[$^{13}C_5$, D_7]-proline in d_8-glycerol/D_2O (60/40) was prepared with 40 mM OX063 as the polarizing agent. Note that the high proline concentration is only necessary for recording the off-signal (no mw) in a reasonable amount of time. Isotopically labeled proline (U-$^{13}C_5$, 97-99 %; U-D_7, 97-99 %; ^{15}N, 97-99 %) was purchased from Cambridge Isotope Laboratories (Andover MA, USA). All solvent mixtures are given in weight ratios.

DNP Spectroscopy

All DNP experiments were performed on a custom-designed DNP NMR spectrometer operating at a magnetic field of 5 T corresponding to a Larmor frequency of 211 MHz (^{1}H) and 140 GHz (e^-), respectively. A custom-designed cryogenic MAS-NMR probe was used for radio-frequency (rf) irradiation (^{13}C and ^{2}H) with a commercial 2.5 mm spinning module (Revolution NMR Inc.). Typically 50 kHz rf field-strength was obtained on the ^{13}C channel, while the ^{2}H field-strength was 83 kHz. ^{2}H-^{13}C cross-polarization was performed using a 50 kHz field on both channels for a duration of 1500 µs. All spectra are recorded without high-power ^{1}H or ^{2}H decoupling (see **Figure 5**).

High-power microwave radiation was generated using a gyrotron oscillator operating at 139.662 GHz [57, 58], capable of producing high-power (>10 W) millimeter waves. The DNP sample (~6 µL) was placed in a 2.5 mm sapphire rotor and a microwave power of 2.5 W was estimated at the position of the sample. The 5 T superconducting magnet is equipped with a superconducting sweep coil to sweep the magnetic field over a range of 750 G. For accurate field measurements, the spectrometer is equipped with a field/frequency lock system[59].

EPR Spectroscopy

EPR experiments were performed on a previously described custom-designed high-field EPR spectrometer operating at a microwave frequency of 139.504 GHz [60, 61]. The sample (~250 nL, 1 mM) was placed in a Suprasil quartz tube with an outer diameter of 0.55 mm. EPR spectra were recorded with a two-pulse echo sequence ($\pi/2$–τ–π–τ–echo) by integrating the echo intensity while sweeping the magnetic field ($t_p(\pi/2)$ = 60 ns, τ = 300 ns). For accurate field measurements, the spectrometer is equipped with a field/frequency lock system[59].

Conclusions

We have demonstrated the application of direct ^{2}H-DNP to two-dimensional ^{2}H, ^{13}C MAS-NMR correlation spectroscopy. A steady-state signal enhancement of ε = 700 was observed with a bulk-polarization build-up constant of τ_B = 21 s. Under these conditions the senistivity of a ^{2}H MAS-NMR experiment can be increased by two orders of magnitude, compared to ^{2}H experiments performed at room temperature. We believe that the combination of perdeuteration and ^{2}H-DNP could have a large impact on protein assignment and structure determination, as the deuteron can be used as an additional nucleus to introduce additional resolution and structural information about the system under study into the spectrum. We believe this approach may be widely applicable, requiring little optimization of isotopic labeling strategies. Furthermore, we expect that technical improvements in hardware and sample preparation for low-temperature MAS-NMR spectroscopy can be expected to vastly improve linewidths in future biological applications. We are currently exploring these improvements.

Acknowledgements

This research was supported by the National Institutes of Health through grants EB002084 and EB002026. TM and LBA acknowledge receipt of a postdoctoral fellowship of the Deutsche Forschungs Gemeinschaft and a graduate research fellowship of the National Science Foundation, respectively. The symmetric trityl radical OX063 was a gift of Nycomed Innovation (now GE Healthcare, Malmo, Sweden). The authors are grateful to Albert Smith, Alexander Barnes, Bjorn Corzilius, and Ta-Chung Ong for many fruitful discussions.

Notes and references

Francis Bitter Magnet Laboratory and Department of Chemistry, Cambridge, 02139 MA, USA. Fax: +1 (617) 253-5404; Tel: +1 (617) 253-5597; E-mail: rgg@mit.edu

† Electronic Supplementary Information (ESI) available: [details of any supplementary information available should be included here]. See DOI: 10.1039/b000000x/

‡ Footnotes should appear here. These might include comments relevant to but not central to the matter under discussion, limited experimental and spectral data, and crystallographic data.

1 A. McDermott, *Annu. Rev. Biophys.*, 2009, **38**, 385-403.

2 C. P. Grey and R. Tycko, *Physics Today*, 2009, **62**, 44-49.

3 D. Zhou, G. Shah, M. Cormos, C. Mullen, D. Sandoz and C. Rienstra, *J. Am. Chem. Soc.*, 2007, **129**, 11791-11801.

4 A. Samoson, T. Tuherm, J. Past, A. Reinhold, T. Anupõld and I. Heinmaa, in *New Techniques in Solid-State NMR*, 2005, pp. 15-31.

5 E. Vinogradov, P. K. Madhu and S. Vega, *Chem. Phys. Lett.*, 2002, **354**, 193-202.

6 A. Lesage, D. Sakellariou, S. Hediger, B. Elena, P. Charmont, S. Steuernagel and L. Emsley, *J. Magn. Reson.*, 2003, **163**, 105-113.

7 V. Agarwal and B. Reif, *J. Magn. Reson.*, 2008, **194**, 16-24.

8 M. Hologne, V. Chevelkov and B. Reif, *Prog. NMR. Spec.*, 2006, **48**, 211-232.

9 V. Agarwal, A. Diehl, N. Skrynnikov and B. Reif, *J. Am. Chem. Soc.*, 2006, **128**, 12620-12621.

10 C. R. Morcombe, E. K. Paulson, V. Gaponenko, R. A. Byrd and K. W. Zilm, *J. Biomol. NMR*, 2005, **31**, 217-230.

11 V. Agarwal, K. Faelber, P. Schmieder and B. Reif, *J. Am. Chem. Soc.*, 2009, **131**, 2-3.

12 C. R. Morcombe, V. Gaponenko, R. A. Byrd and K. W. Zilm, *J. Am. Chem. Soc.*, 2005, **127**, 397-404.

13 S. Vega, T. W. Shattuck and A. Pines, *Phys. Rev. Lett.*, 1976, **37**, 43.

14 A. Hoffman and I. Schnell, *ChemPhysChem*, 2004, **5**, 966-974.

15 T. Maly, G. T. Debelouchina, V. S. Bajaj, K.-N. Hu, C.-G. Joo, M. L. MakJurkauskas, J. R. Sirigiri, P. C. A. van der Wel, J. Herzfeld, R. J. Temkin and R. G. Griffin, *J. Chem. Phys.*, 2008, **128**, 052211-052219.

16 A. Barnes, M. L. Mak-Jurkauskas, Y. Matsuki, V. S. Bajaj, P. C. A. van der Wel, R. DeRocher, J. Bryant, J. R. Sirigiri, R. J. Temkin, J. Lugtenburg, J. Herzfeld and R. G. Griffin, *J. Magn. Reson.*, 2009, **198**, 261-270.

17 S. T. Goertz, *Nucl. Instrum. Methods Phys. Res., Sect. A*, 2004, **526**, 28-42.

18 R. A. Wind, M. J. Duijvestijn, C. van der Lugt, A. Manenschijn and J. Vriend, *Prog. NMR. Spec.*, 1985, **17**, 33-67.

19 F. A. Gallagher, M. I. Kettunen, S. E. Day, D.-E. Hu, J. H. Ardenkjaer-Larsen, R. i. t. Zandt, P. R. Jensen, M. Karlsson, K. Golman, M. H. Lerche and K. M. Brindle, *Nature*, 2008, **453**, 940-943.

20 I. J. Day, J. C. Mitchell, M. J. Snowden and A. L. Davis, *Appl. Magn. Reson.*, 2008, **34**, 453-460.

21 A. B. Barnes, G. De Paëpe, P. C. A. van der Wel, K. N. Hu, C. G. Joo, V. S. Bajaj, M. L. Mak-Jurkauskas, J. R. Sirigiri, J. Herzfeld, R. J. Temkin and R. G. Griffin, *Appl. Magn. Reson.*, 2008, **34**, 237-263.

22 V. S. Bajaj, M. L. Mak-Jurkauskas, M. Belenky, J. Herzfeld and R. G. Griffin, *Proc. Nat. Aca. Sci. USA*, 2009, -.

23 K. Hu, H. Yu, T. Swager and R. Griffin, *J. Am. Chem. Soc.*, 2004, **126**, 10844-10845.

24 C. T. Farrar, D. A. Hall, G. J. Gerfen, S. J. Inati and R. G. Griffin, *J. Chem. Phys.*, 2001, **114**, 4922-4933.

25 V. A. Atsarkin, *Sov. Phys. Usp. (english translation)*, 1978, **21**, 725-743.

26 D. S. Wollan, *Phys. Rev. B*, 1976, **13**, 3686.

27 D. S. Wollan, *Phys. Rev. B*, 1976, **13**, 3671.

28 N. Bloembergen, *Physica*, 1949, **15**, 386-426.

29 M. Borghini and K. Scheffler, *Nuc. Inst. and Methods*, 1971, **95**, 93-98.

30 M. Borghini, A. Masaike, K. Scheffler and F. Udo, *Nuc. Inst. and Methods*, 1971, **97**, 577-579.

31 S. T. Goertz, J. Harmsen, J. Heckmann, C. He, W. Meyer, E. Radtke and G. Reicherz, *Nucl. Instrum. Methods Phys. Res., Sect. A*, 2004, **526**, 43-52.

32 S. Reynolds and H. Patel, *Appl. Magn. Reson.*, 2008, **34**, 495-508.

33 O. Y. Grinberg, A. A. Dubinskii and Y. S. Lebedev, *Russ. Chem. Rev.*, 1983, **52**, 850-865.

34 J. Wolber, F. Ellner, B. Fridlund, A. Gram, H. Johannesson, G. Hansson, L. H. Hansson, M. H. Lerche, S. Mansson, R. Servin, M. Thaning, K. Golman and J. H. Ardenkjaer-Larsen, *Nucl. Instrum. Methods Phys. Res., Sect. A*, 2004, **526**, 173-181.

35 C. D. Jeffries, *Physical Review Phys. Rev. PR*, 1960, **117**, 1056.

36 A. Abragam and M. Goldman, *Nuclear magnetism : order and disorder*, Clarendon Press Oxford University Press, Oxford New York, 1982.

37 A. Abragam and M. Goldman, *Rep. Prog. Phys.*, 1978, **41**, 395-467.

38 C. Song, K. Hu, C. Joo, T. Swager and R. Griffin, *J. Am. Chem. Soc.*, 2006, **128**, 11385-11390.

39 Y. Matsuki, T. Maly, O. Ouari, H. Karoui, F. Moigne Le, E. Rizzato, S. Lyubenova, J. Herzfeld, T. F. Prisner, P. Tordo and R. G. Griffin, *Angew. Chem. Int. Ed.*, 2009, **48**, 4996-5000.

40 T. Maly, A.-F. Miller and R. G. Griffin, *ChemPhysChem*, 2010.

41 K.-N. Hu, C. Song, H.-h. Yu, T. M. Swager and R. G. Griffin, *J. Chem. Phys.*, 2008, **128**, 052302-052317.

42 T. Reddy, T. Iwama, H. Halpern and V. Rawal, *J. Org. Chem.*, 2002, **67**, 4635-4639.

43 M. Bowman, C. Mailer and H. Halpern, *J. Magn. Reson.*, 2005, **172**, 254-267.

44 C. F. Koelsch, *J. Am. Chem. Soc.*, 1957, **79**, 4439-4441.

45 J. Ardenkjær-Larsen, B. Fridlund, A. Gram, G. Hansson, L. Hansson, M. Lerche, R. Servin, M. Thaning and K. Golman, *Proc. Nat. Aca. Sci. USA*, 2003, **100**, 10158-10163.

46 M. Glyavin, V. Khizhnyak, A. Luchinin, T. Idehara and T. Saito, *International Journal of Infrared and Millimeter Waves*, 2008, **29**, 641-648.

47 M. K. Hornstein, V. S. Bajaj, R. G. Griffin, K. E. Kreischer, I. Mastovsky, M. A. Shapiro, J. R. Sirigiri and R. J. Temkin, *IEEE Transactions on Electron Devices*, 2005, **52**, 798-807.

48 A. C. Torrezan, S.-T. Han, I. Mastovsky, M. Shapiro, J. R. Sirigiri, R. J. Temkin, A. Barnes and R. G. Griffin, *IEEE Transactions on Plasma Science*, accepted for publication.

49 A. Pines, M. G. Gibby and J. S. Waugh, *J. Chem. Phys.*, 1972, **56**, 1776-1777.

50 A. E. Bennett, C. M. Rienstra, M. Auger, K. V. Lakshmi and R. G. Griffin, *J. Chem. Phys.*, 1995, **103**, 6951-6958.

51 A. Pines, M. G. Gibby and J. S. Waugh, *J. Chem. Phys.*, 1973, **59**, 569-590.

52 N. Chandrakumar, G. v. Fircks and Harald G¸nther, *Magn. Reson. Chem.*, 1994, **32**, 433-435.

53 K. Warncke, G. T. Babcock and J. McCracken, *J. Phys. Chem.*, 1996, **100**, 4654-4661.

54 P. van der Wel, K. Hu, J. Lewandowski and R. Griffin, *J Am Chem Soc*, 2006, **128**, 10840-10846.

55 A. Barnes, *Personal communication*, 2010.

56 S. Mamone, A. Dorsch, O. G. Johannessen, M. V. Naik, P. K. Madhu and M. H. Levitt, *J. Magn. Reson.*, 2008, **190**, 135-141.

57 L. Becerra, G. Gerfen, R. Temkin, D. Singel and R. Griffin, *Phys. Rev. Lett.*, 1993, **71**, 3561-3564.

58 V. L. Granatstein, R. K. Parker and C. M. Armstrong, *Proc. IEEE*, 1999, **87**, 702-716.

59 T. Maly, J. Bryant, D. Ruben and R. Griffin, *J. Magn. Reson.*, 2006, **183**, 303-307.

60 M. Bennati, C. Farrar, J. Bryant, S. Inati, V. Weis, G. Gerfen, P. Riggs-Gelasco, J. Stubbe and R. Griffin, *J. Magn. Reson.*, 1999, **138**, 232-243.

61 L. R. Becerra, G. J. Gerfen, B. F. Bellew, J. A. Bryant, D. A. Hall, S. J. Inati, R. T. Weber, S. Un, T. F. Prisner, A. E. McDermott, K. W. Fishbein, K. Kreischer, R. J. Temkin, D. J. Singel and R. G. Griffin, *J. Magn. Reson.*, 1995, **A117**, 28-40.